Author Manuscript Author Manuscript Author Manuscript Author Manuscript

HHS Public Access
Author manuscript
IEEE Appl Imag Pattern Recognit Workshop. Author manuscript; available in PMC 2017 November 16.

Published in final edited form as:
IEEE Appl Imag Pattern Recognit Workshop. 2016 October ; 2016: .

Confocal Vessel Structure Segmentation with Optimized Feature Bank and Random Forests

Yasmin M. Kassim[*], **V. B. Surya Prasath**[*], **Olga V. Glinskii**[†,‡], **Vladislav V. Glinsky**[†,§], **Virginia H. Huxley**[‡,¶], and **Kannappan Palaniappan**[*]

[*]Computational Imaging and VisAnalysis (CIVA) Lab Department of Computer Science, University of Missouri-Columbia, Columbia, MO 65211 USA

[†]Research Service, Harry S. Truman Memorial Veterans Hospital, Columbia, MO 65201 USA

[‡]Department of Medical Pharmacology and Physiology, University of Missouri-Columbia, Columbia, MO 65211 USA

[§]Department of Pathology and Anatomical Sciences, University of Missouri-Columbia, Columbia, MO 65211 USA

[¶]National Center for Gender Physiology, University of Missouri-Columbia, MO 65211 USA

Abstract

In this paper, we consider confocal microscopy based vessel segmentation with optimized features and random forest classification. By utilizing multi-scale vessel-specific features tuned to capture curvilinear structures such as Frobenius norm of the Hessian eigenvalues, Laplacian of Gaussians (LoG), oriented second derivative, line detector and intensity masked with LoG scale map. we obtain better segmentation results in challenging imaging conditions. We obtain binary segmentations using random forest classifier trained on physiologists marked ground-truth. Experimental results on mice dura mater confocal microscopy vessel segmentations indicate that we obtain better results compared to global segmentation approaches.

1. Introduction

Vasculature segmentation is an important requirement in many biomedical imaging domains such as microscopy, angiography, and optical fundoscopy. Various vessel segmentation methods has been considered in the past [1], [2], [3], [4], [5], see [6] for a review. Many of these methods rely on global or local intensity features and have limitations in terms of detecting thin vascular structures present fluorescence or confocal microscopy images. Confocal microscopy contains spatially varying noise and relying purely on intensity features alone without any learning approach can often lead to poor results in terms of capturing thin vessels and spatial continuity, see Figure 1 where we show a comparison of intensity based thresholding methods. As can be seen by comparing with ground-truth (GT), the intensity features based segmentation methods miss important vessel segmentations and also obtain spurious foreground pixels.

Author Manuscript Author Manuscript Author Manuscript Author Manuscript

To avoid these drawbacks, in [7] we used a set of vessel specific optimized features along with random forest (RF) classifier based segmentation for robust curvilinear structure extraction from epifluorescence imagery under challenging imaging conditions. In this work, we extend our work in [7] by utilizing intensity based Laplacian of Gaussian (LoG) for capturing the spatial variations which are unique to confocal imagery. Due to the nature of confocal imaging where local intensity information is important, adding a multiscale LoG based intensity feature improves the final segmentation accuracy. Experimental results on a set of confocal microscopy imagery of mice dura mater micro-vessel segmentation show that our proposed RF based approach obtains better results compared to global thresholding methods from the literature. Moreover, by comparing with manually annotated GT vessel structures our proposed approach obtained better quantitative results indicating high fidelity results.

We organized the rest of the paper as follows. Section 2 details the optimized features utilized in random forest based classification for confocal vessel segmentations. Section 3 provides detailed experimental results on a set of confocal imagery along with comparisons of other global segmentation methods. Finally, Section 4 concludes the paper.

2. Optimized Feature Bank for Random Forest Classifier Based Segmentation

We use random forest (RF) classifier [8] based approach which is adapted for vessel structure and cell segmentation with high precision and recall [7], [9]. Our feature bank is optimized to capture curvilinear structures of varying width as well robust to scale changes. We next describe in detail the optimized feature bank which is devised to obtain better vessel structure segmentations from confocal imagery.

2.1. Vessel specific optimized feature bank

We chose a particular set of features which are fine-tuned to obtain optimal vessel differentiability from background. They are based on Hessian eigenvalues based multiscale Frobenius norms, multiscale Laplacian of Gaussians (LoG), a multiscale line detector [2]. Here we provide the basic details of each of these features and refer to [7] more details of these optimized feature bank for vessel segmentation.

- *Frobenius norm of the Hessian matrix (6-D)*: A second order vessel *structureness* term was initially defined by Frangi et al [1]. The second derivative Hessian operator $\mathcal{H}_\sigma$ is useful for detecting ridges, valleys and peaks. The Frobenius norm of the multiscale Hessian matrix usually has small values in the background where there are no strong linear or blob-like features; the maximum eigenvalue will be large in the foreground regions containing vessel-like structures. The eigenvalues are transformed using the hyperbolic tangent function:

$$\tilde{\lambda}_{\pm}(\sigma)=\frac{1-\exp\left(-|\lambda_{\pm}|\right)}{1+\exp\left(-|\lambda_{\pm}|\right)}. \quad (1)$$

We use these transformed eigenvalues from the Frobenius norm at a scale σ,

$$\|\mathscr{H}_\sigma\|_F=\sqrt{\tilde{\lambda}_+^2+\tilde{\lambda}_-^2} \quad (2)$$

We calculate the Frobenius norm (2) using scale normalized Gaussian filters for five scales, $\sigma = \{1, 2, 3, 4, 5\}$[1]. Additionally, we utilize the maximum response of the regular Frobenius norm ($\|\mathscr{H}_\sigma\|_F$) of the Hessian across five scales followed by z-score sigmoid normalization.

- *Oriented second derivatives (6-D)& Laplacian of Gaussian (LoG) filters (2-D)*: We used multiscale filters consisting of 18 oriented second derivative (6 orientation, 3 scale, mean normalized) and 8 isotropic LoG filters. We used the maximum response of the 6 oriented second derivative filters over 3 scales ($\sigma=\{\sqrt{2},2,2\sqrt{2}\}$). Further, the scale specific orientation feature is included for each pixel and assigns a discrete orientation angle index/label corresponding to the maximum filter response. Two LoG-based features are the maximum response over 8 scales ($\sigma=\{\sqrt{2},2,2\sqrt{2},4\}$ and 3σ) and the corresponding scale index.

- *Multiscale line detector (1-D)*: The multiscale line detector feature is based on the approach of Nguyen et al [2]. This method uses 12 oriented lines sampled regularly between 0 to 360 degrees. By varying the length parameter we can generate lines of different scales which can detect different diameter vessels. We select the window size (W) to be 15 and the range of length L in {3, 5, 7, 9, 11, 13, 15}.

Table 1 summarizes the optimized feature bank which are used as 15 dimensional input vector to the RF classifier based segmentation approach. Figure 2 shows features computed for an example confocal image (20 × 11). In addition to these 15 features we utilize a novel intensity driven multiscale LoG scale-map feature that captures vessels in confocal imagery where the contrast is varying widely and eliminate the noisy background:

- *LoG with intensity*: We consider the scale map of LoG maximum response computed over 8 scales and multiply it by the input image's intensity fellowed by z-score normalization. This feature captures multi-scale vessel structures and regions where the contrast is low and eliminate the noisy background. Figure 3 shows an example result of this feature for image 20 × 21. As can be seen in Figure 3(c), the noisy background has been eliminated by this feature.

In our experiments we found that adding this extra feature increased the accuracy by 7% over RF-15 and 3% over RF-16, see Section 3.2 and Table 2. The intuition from this table is to show that adding the intensity in a smart way lead to improve the performance and overcome the drawbacks of the noisy background.

[1]Each scale uses a filtering window size of $[-3\sigma, 3\sigma]$

Author Manuscript Author Manuscript Author Manuscript Author Manuscript

2.2. Random forests classification for vessel segmentations

The RF classifier was used with a total of 24 mice dura mater confocal microscopy images with pixel dimensions 1024 × 1024. We use three-fold cross validation to get the results, the dataset has been randomly split in to three sets; each time we train one set to get the prediction of the other two. As a result, each image has two values from different tests, the results have been calculated by averaging the two values. For each experiment, the dimensionality of the feature vector is 16 dimensions with 8, 388, 608 observations. We used manually labeled ground-truth (GT) segmentations of the microvasculature images supervised by an expert physiologist for pixel-based training using the gray scale images.There is neither preprocessing nor post processing to generate the results.

3. Experimental Results

3.1. Setup and parameters

We utilized a set of 24 at different resolutions (10×, 20×, 20×, 40×) confocal stacks obtained with a IX-70 Olympus (inverted) microscope with Solamere confocal unit and 2 camera (B&W and ultra low Mega-10). We applied a multiscale focus fusion method [4] to obtain fused confocal images which are then utilized as input images to automatic segmentation methods. To quantitatively compare the automatic segmentation methods we use the Dice coefficient,

$$Dice(A, B)=\frac{2|A\cap B|}{|A|+|B|}, \quad (3)$$

where A and B are the pixel level automatic and GT segmentations. Dice values closer to one indicate better performance compared to the physiologist expert verified gold standard segmentations.

3.2. Effect of intensity LoG feature in RF segmentation

Table 2 shows the effect of intensity feature in our RF classifier based segmentation approach. We show RF-intensity which is based only on intensity feature, RF-15 using 15 features described in Table 1 (see also Figure 2, Section 2.1), RF-16 with intensity, and RF-16-LoG which includes the multiscale LoG with intensity feature (see Figure 3). Figure 5 shows comparison of segmentations between these different RF variations. Overall, it can be seen that the RF-16-LoG obtained best possible results across most input images indicating that vessel specific optimized feature bank augmented with LoG with intensity feature has better vessel discriminative power, see Table 2 last column.

3.3. Comparison results

We compare our RF classifier based segmentation approach with Niblack and Otsu which are intensity based thresholding and segmentation methods. Extensive parameter sweeping was used to search for the optimal Otsu and Niblack segmentation parameters like local window size and threshold. Table 3 shows the Dice values obtained with Niblack, Otsu and

Author Manuscript Author Manuscript Author Manuscript Author Manuscript

Author Manuscript
Author Manuscript
Author Manuscript
Author Manuscript

our proposed RF classifier based segmentation approaches. As can be seen, the proposed method obtained higher Dice, and accuarcy values indicating superior performance. In addition, we calculate the average sensitivity, specificity and accuracy and show in Figure 4. We note that though both Niblack and Otsu methods obtained high specificity values their sensitivity values are ver low. This is due to the fact that both of these methods miss a lot vessel foreground pixels (true negative). Figure 6 shows three example segmentation results with manual GT, Otsu, Niblack [3]) and our RF classifier based segmentation methods. We obtain good vessel segmentations with segmenting the low intensity regions that have been missed in Niblack and Otsu represented by red color.

4. Conclusions

In this paper, we considered micro-vessel segmentation from confocal microscopy images using vessel-specific feature bank and random forest classifier. By combining multiscale, multi orientation features with intensity masked by LoG scale map we obtain a reliable bank of features which are then utilized for foreground-background segmentation of vasculature images. Random forest was trained using a set of ground-truth segmentations provided by the expert physiologist which in turn provided accurate classification results. Experimental results on a set of different resolution confocal microscopy images of mice dura mater in the brain shows that we obtain better results when compared to other global segmentation methods. Currently we are working on utilizing an anisotropic diffusion based vessel smoothing and enhancing filter [10] prior to random forest classification.

Acknowledgments

This research was supported in part by the Award #1I01BX000609 from the Biomedical Laboratory Research & Development Service of the VA Office of Research and Development (VVG), the National Cancer Institute of the National Institutes of Health Award #R01CA160461 (VVG) and #R33EB00573 (KP).

References

1. Frangi AF, Niessen WJ, Vincken KL, Viergever MA. Multiscale vessel enhancement filtering. Lecture Notes in Computer Science (MICCAI). 1998; 1496:130–137.
2. Nguyen UTV, Bhuiyan A, Park LAF, Ramamohanarao K. An effective retinal blood vessel segmentation method using multiscale line detection. Pattern Recognition. 2013; 46(3):703–715.
3. Prasath, VBS., Bunyak, F., Haddad, O., Glinskii, O., Glinskii, V., Huxley, V., Palaniappan, K. Robust filtering based segmentation and analysis of dura mater vessels using epifluorescence microscopy. 35th IEEE/EMBS International Conference; Osaka, Japan. July 2013; p. 6055-6058.
4. Pelapur, R., Prasath, VBS., Bunyak, F., Glinskii, OV., Glinsky, VV., Huxley, VH., Palaniappan, K. Multi-focus image fusion on epifluorescence microscopy for robust vascular segmentation. 36th IEEE/EMBS International Conference; Chicago, USA. August 2014; p. 4735-4738.
5. Meena, S., Prasath, VBS., Kassim, YM., Maude, RJ., Glinskii, OV., Glinsky, VV., Huxley, VH., Palaniappan, K. Multiquadrics based interactive segmentation of dura mater microvasculature from epifluorescence images," in. 36th IEEE/EMBS International Conference; Florida, USA. August 2016; p. 5913-5916.
6. Kirbas C, Quek F. A review of vessel extraction techniques and algorithms. ACM Computing Surveys. 2004; 36(2):81–121.
7. Kassim, YM., Prasath, VBS., Pelapur, R., Glinskii, OV., Maude, RJ., Glinsky, VV., Huxley, VH., Palaniappan, K. Random forests for dura mater microvasculature segmentation using

epifluorescence images. 36th IEEE/EMBS International Conference; Florida, USA. August 2016; p. 2901-2904.

8. Breiman L. Random forests. Machine Learning. 2001; 45(1):5–32.
9. Prasath, VBS., Kassim, YM., Oraibi, ZA., Guiriec, J-B., Hafiane, A., Palaniappan, K. HEp-2 cell classification and segmentation using motif texture patterns and spatial features with random forests. Proc. IEEE International Conference on Pattern Recognition (ICPR); Dec 2016;
10. Prasath, VBS., Pelapur, R., Glinskii, OV., Glinsky, VV., Huxley, VH., Palaniappan, K. Multi-scale tensor anisotropic filtering of fluorescence microscopy for denoising microvasculature. IEEE International Symposium on Biomedical Imaging (ISBI); NewYork, USA. April 2015; p. 540-543.

Author Manuscript Author Manuscript Author Manuscript Author Manuscript

Author Manuscript
Author Manuscript
Author Manuscript
Author Manuscript

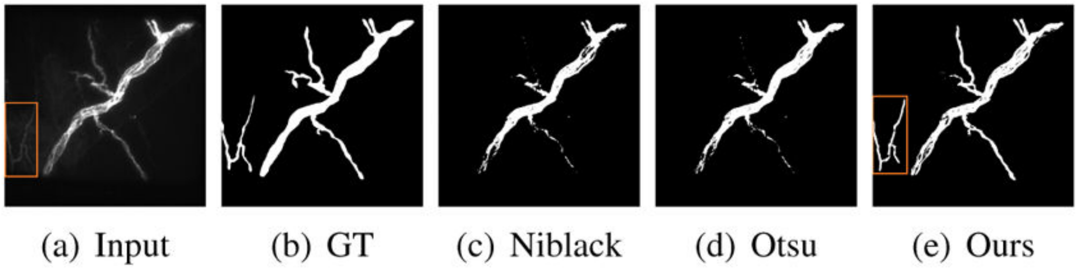

Figure 1.
We obtain robust, and higher precision vessel segmentations when compared to other purely intensity based segmentation methods. (a) Input confocal image (10× resolution, contrast enhanced for visualization), (b) Ground-truth (GT) marked by an experienced physiologist, and automatic segmentation results from, (c) Niblack (Dice 0.7156), (d) Otsu (Dice 0.7538), and (e) our proposed random forest (RF) classifier based approach (Dice 0.8710). Our method was able to capture vessel branches with low texture content in contrast to Niblack and Otsu methods, see the boxed regions in (a) and (e).

Author Manuscript Author Manuscript Author Manuscript Author Manuscript

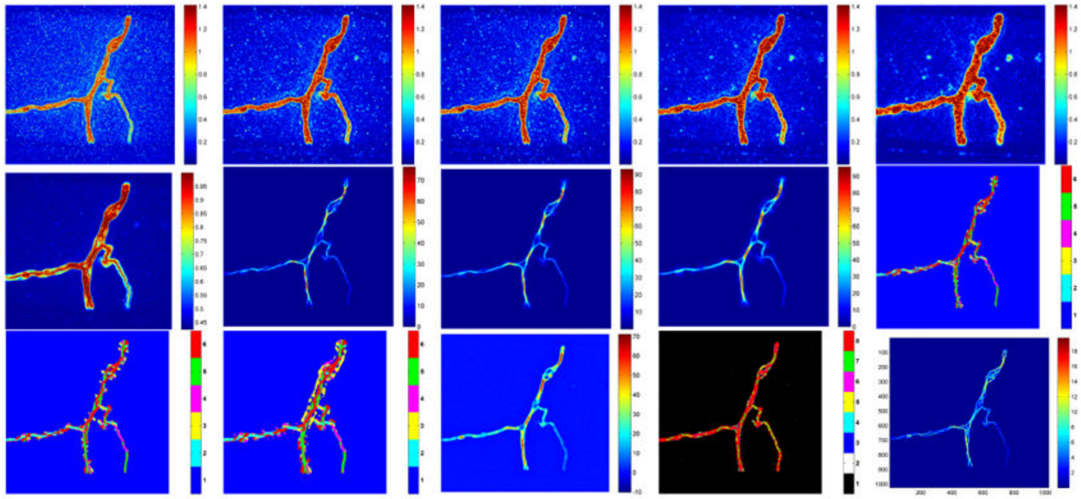

Figure 2.

The 15 vessel specific features (shown here for image 20 × 11) used in the random forest classifier are: Frobenius norm of Hessian (2) at 5 scales and its sigmoid scale map, maximum response of second derivatives at 3 scales over 6 orientations and orientation maps (30 deg steps), maximum response of Laplacian of Gaussian (LoG) at 8 scales and its sigma scale map, and response of the multiscale line detector, see Table 1.

Author Manuscript Author Manuscript Author Manuscript Author Manuscript

(a) Input (b) LoG scale map (c) LoG+intensity

Figure 3.

Advantage of multiscale LoG scale map with intensity. (a) Input image (20x−21), (b) LoG scale map computed at eight scales with dice value 0.8037 whereas the final segmentation for the proposed approach for this image is 0.8768 as shown in Table 2. (c) LoG scale map masked with intensity. This feature succeeds in capturing multiscale vessel structures and regions where the contrast is not high in addition to filter out the noisy background.

Author Manuscript
Author Manuscript
Author Manuscript
Author Manuscript

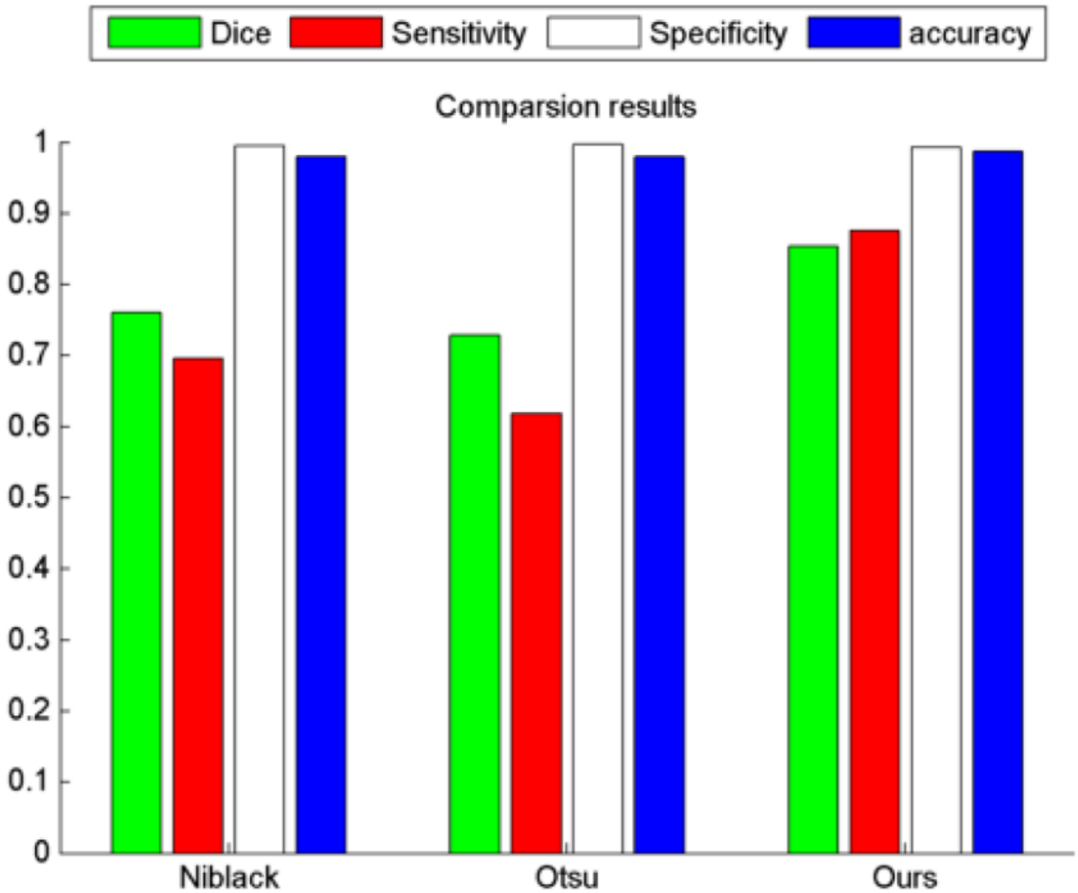

Figure 4.
Comparison of global methods Niblack, and Otsu with our RF-16-LoG approach on confocal images in terms of different error metrics.

Author Manuscript Author Manuscript Author Manuscript Author Manuscript

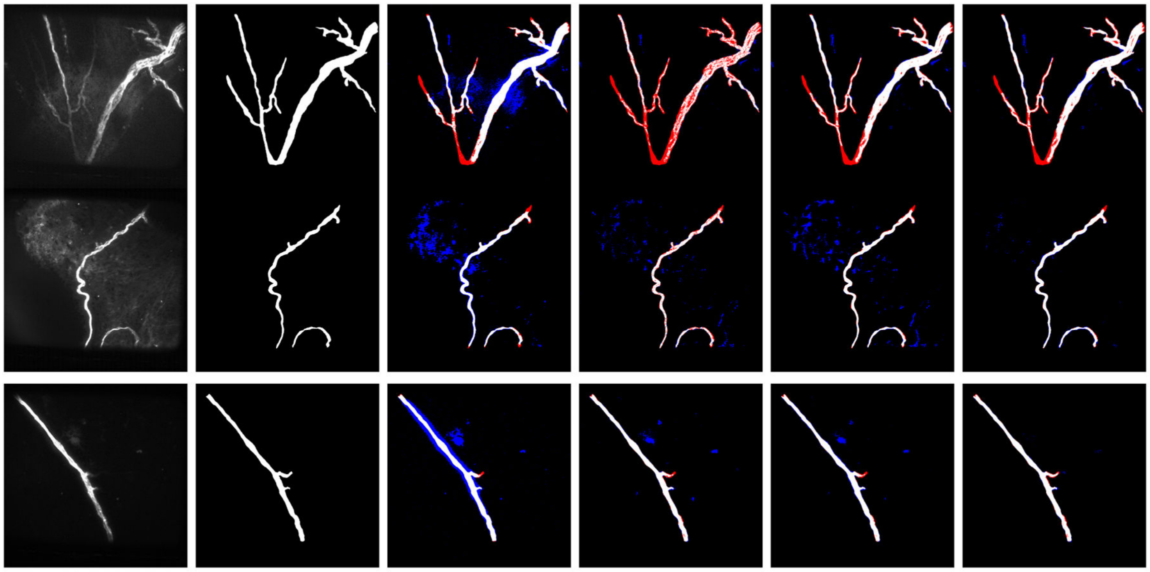
(a) Input (b) GT (c) RF-intensity (d) RF-15 (e) RF-16 (f) RF-16-LoG

Figure 5.

Comparison of variations of our RF approach on different confocal images. Top to bottom: 20x−15, 20x−21, and 20x−8. (a) Input confocal images (contrast enhanced for visualization), (b) ground-truth (GT) images marked by an experienced physiologist, (c) random forest with only intensity (RF-intensity) with dice values equal to **0.7314**, **0.5937** and **0.6128**, (d) RF with all features except intensity (RF-15) with dice values equal to **0.6603**, **0.7129** and, **0.8826**, and (e) RF with all features in addition to intensity (RF-16) with dice values equal to **0.8284**, **0.6774** and **0.8804**. White regions represent correctly segmented pixels, red are missing (false negative) and blue are extra regions (false positive) compared to ground truth. (f) RF with all features in addition to intensity masked with LoG scale map (RF-16-LoG) with dice values equal to **0.8548**, **0.8768** and **0.9332**. White regions represent correctly segmented pixels, red are missing (false negative) and blue are extra regions (false positive) compared to ground truth.

Author Manuscript Author Manuscript Author Manuscript Author Manuscript

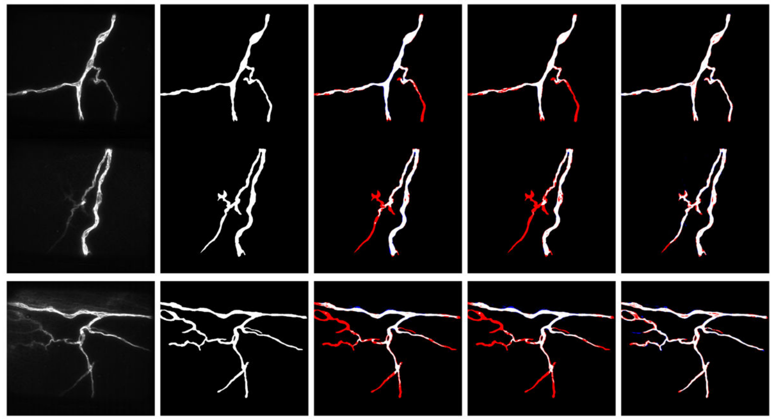

Figure 6.

Comparison of global methods with our RF approach on different confocal images. Top to bottom: 20x−11, 20x−1, 20x−19. (a) Input confocal images (contrast enhanced for visualization), (b) ground-truth (GT) images marked by an experienced physiologist, and and automatic segmentation results from (c) Niblack with dice values 0.8687, 0.8552,and 0.7042, (d) Otsu with dice values 0.8315, 0.7962, and 0.7030, (e) our proposed RF-16 with dice values **0.9351**, **0.8871**, and **0.8905**. White regions represent correctly segmented pixels, red are missing (false negative) and blue are extra regions (false positive) compared to ground-truth.

Author Manuscript
Author Manuscript
Author Manuscript
Author Manuscript

TABLE 1

Description and dimensionality of the input feature vector for the random forest (RF) classifier (see Figure 2).

Feature	Dim.
Modified Frobenius norm over 5 scales & max scale regular Frobenius	6
Maximum response of oriented 2nd derivatives over 3 scales & 3 orientation maps	6
Maximum response over eight scales of LoG filter & sigma map	2
Multiscale Line Detector	1

Author Manuscript Author Manuscript Author Manuscript Author Manuscript

TABLE 2

Comparison of RF classifier based segmentation approach with different combination of features. We show Dice values for RF-Intensity based only on intensity feature, RF-15 using 15 features given in Table 1 except the intensity feature, RF-16 with the intensity feature and RF-16-LoG is the full feature set with intensity masked with LoG scale map mask.

No.	Image	RF-Intensity	RF-15	RF-16	RF-16-LoG
1	10 × 1	0.4689	0.6530	**0.7672**	0.7126
2	20 × 1	0.8240	0.8234	0.8398	**0.8871**
3	20 × 2	0.6076	0.7615	0.7710	**0.8032**
4	20 × 3	0.7451	0.7885	0.7814	**0.8521**
5	20 × 4	0.8286	0.8686	0.8716	**0.8725**
6	20 × 5	0.8521	0.8607	0.8771	**0.8915**
7	20 × 6	0.6621	0.7514	0.7544	**0.8237**
8	20 × 7	0.7050	0.8162	0.8651	**0.9102**
9	20 × 8	0.6128	0.8826	0.8804	**0.9332**
10	20 × 9	0.7485	0.8180	0.8273	**0.8625**
11	20 × 10	0.7460	**0.9009**	0.8936	0.8808
12	20 × 11	0.8827	0.8625	**0.9365**	0.9351
13	20 × 12	0.7620	0.8323	0.8290	**0.8628**
14	20 × 13	0.8195	0.8545	0.8637	**0.8974**
15	20 × 14	0.8349	0.8353	0.8565	**0.8752**
16	20 × 15	0.7314	0.6603	0.8284	**0.8548**
17	20 × 16	0.7760	0.8031	0.8108	**0.8203**
18	20 × 17	0.5908	0.7669	0.7678	**0.8074**
19	20 × 18	0.7030	0.7893	0.7919	**0.8327**
20	20 × 19	0.7562	0.7698	0.8455	**0.8905**
21	20 × 20	0.5461	0.7755	0.7594	**0.7967**
22	20 × 21	0.5937	0.7129	0.6774	**0.8768**
23	20 × 22	0.6900	0.7936	0.7932	**0.8393**
24	40 × 1	0.5284	0.4991	0.8305	**0.8716**
Avg.		0.7090	0.7867	0.8216	**0.8579**

Author Manuscript

Author Manuscript

Author Manuscript

Author Manuscript

TABLE 3

Comparison of automatic segmentation methods on confocal microscopy images of mice dura mater. We show the Dice values for our proposed random forest approach, compared with Niblack [3], and Otsu thresholding methods. Higher Dice values indicate better results when compared to the manual gold-standard ground-truth segmentations.

No.	Image Res.	Niblack	Otsu	Ours
1	10 × 1	0.7390	**0.7541**	0.7126
2	20 × 1	0.8552	0.7962	**0.8871**
3	20 × 2	0.6842	0.7187	**0.8032**
4	20 × 3	0.7699	0.7046	**0.8521**
5	20 × 4	0.7821	0.7625	**0.8725**
6	20 × 5	0.8532	0.8223	**0.8915**
7	20 × 6	0.7095	0.6318	**0.8237**
8	20 × 7	0.8322	0.6544	**0.9102**
9	20 × 8	0.8934	0.8596	**0.9332**
10	20 × 9	0.7304	0.6894	**0.8625**
11	20 × 10	0.7224	0.7123	**0.8808**
12	20 × 11	0.8687	0.8315	**0.9351**
13	20 × 12	0.7300	0.6769	**0.8628**
14	20 × 13	0.8161	0.7475	**0.8974**
15	20 × 14	0.7156	0.7538	**0.8752**
16	20 × 15	0.7051	0.7625	**0.8548**
17	20 × 16	0.7180	0.6949	**0.8203**
18	20 × 17	0.6421	0.6631	**0.8074**
19	20 × 18	0.6452	0.4907	**0.8327**
20	20 × 19	0.7042	0.7030	**0.8905**
21	20 × 20	**0.8112**	0.7627	0.7967
22	20 × 21	0.7995	0.7909	**0.8768**
23	20 × 22	0.7430	0.7468	**0.8393**
24	40 × 1	0.7772	0.7567	**0.8716**
Avg.		0.7603	0.7286	**0.8579**
Avg.	Sensitivity	69.6105	61.8451	**87.5669**
Avg.	Specificity	99.5039	**99.6366**	99.2003
Avg.	Accuracy	97.9717	97.8936	**98.7032**